Physics Letters B 812 (2021) 136025

Contents lists available at ScienceDirect

Physics Letters B

www.elsevier.com/locate/physletb

Shadows of 5D black holes from string theory

A. Belhaj [a], H. Belmahi [a], M. Benali [a], W. El Hadri [a], H. El Moumni [b], E. Torrente-Lujan [c,*,1]

[a] Département de Physique, Équipe des Sciences de la matière et du rayonnement, ESMaR, Faculté des Sciences, Université Mohammed V de Rabat, Rabat, Morocco
[b] EPTHE, Physics Department, Faculty of Science, Ibn Zohr University, Agadir, Morocco
[c] IFT, Dep. de Física, Universidad de Murcia, Campus de Espinardo, E-30100 Murcia, Spain

ARTICLE INFO

Article history:
Received 5 October 2020
Received in revised form 22 November 2020
Accepted 10 December 2020
Available online 15 December 2020
Editor: N. Lambert

Keywords:
Black holes
Shadows
D3-branes
Type IIB superstring theory

ABSTRACT

We study the shadow behaviors of five dimensional (5D) black holes embedded in type IIB superstring/supergravity inspired spacetimes by considering solutions with and without rotations. Geometrical properties as shapes and sizes are analyzed in terms of the D3-brane number and the rotation parameter. Concretely, we find that the shapes are indeed significantly distorted by such physical parameters and the size of the shadows decreases with the brane or "color" number and the rotation. Then, we investigate geometrical observables and energy emission rate aspects.

Contents

1. Introduction

Black holes have been extensively investigated in connections with many gravity theories. Such investigations have been boosted by recent direct observations, the gravitational wave events and by the first image provided by the Event Horizon telescope (EHT) international collaboration [1–4]. From this observation, it has been induced the diameter of the central black hole shadow which is $(42 \pm 3)\mu as$ with a deviation $< 10\%$ from circularity. This leads to a estimation of the center mass, given by $M = (6.5 \pm 0.7) \times 10^9 M_\odot$, under Einstein General Relativity (GR). This is an example of how these and future observations could provide a window to explore the strong gravity regime and distinguish amog models.

The black hole shadow is nothing but a two-dimensional dark zone in the celestial sphere caused by the strong gravitational lensing of lights near these compact objects. It has been shown that the shape and the size of the shadow, being controlled by many parameters,

* Corresponding author.
E-mail addresses: belhajadil@fsr.ac.ma (A. Belhaj), hajar.smp.belmahi987@gmail.com (H. Belmahi), mohamed_benali4@um5.ac.ma (M. Benali), elhadriwijdane4@gmail.com (W. El Hadri), hasan.elmoumni@edu.uca.ma (H. El Moumni), torrente@cern.ch (E. Torrente-Lujan).
[1] Authors in alphabetical order.

https://doi.org/10.1016/j.physletb.2020.136025

rely on the geometry of the spacetime in which black holes live. Such observational data can provide significative information regarding the black hole spacetime and the associated gravitation theory. In this context, several works have dealt with the shadow of various black holes using appropriate tools and methods. In particular, an interplay between the quasi-normal modes of the black hole and its shadow has been investigated in [5,6]. Moreover, the influence of non-trivial matter fields on such optical behaviors has been reported in [7,8].

Thermodynamical and other optical aspects of black holes, in $4D$ and arbitrary dimensions, have been treated using different approaches and methods including numerical ones [9–21]. Concretely, some studies have focused on a link between black holes on Anti-de-Sitter (AdS) geometries with a negative cosmological and theromodynamical models. Interpreting the cosmological constant as the pressure and its conjugate as the volume, a bridge between the behaviors of RN-AdS black holes and the behavior of Van der Waals fluids has been established. In particular, it has been revealed that PV criticality can be related liquid-gas statistical systems. Such aspects have been also investigated using shadow formalism [21]. Moreover, black hole objects living in higher dimensions, involving various rotating parameters required by space-time symmetries, have been also studied. In such spaces, non-trivial extended compact objects can also arise going beyond black holes supported by brane physics. The associated horizon geometries have been obtained and examined with using alternative ways.

Many other physical properties have been shown in connections with non-trivial models of gravity in extra dimensions. Specifically, string theory motivated models have been used as playgrounds to study certain phase transitions of black holes in the presence of solitonic D-brane objects. Precisely, the Hawking-Page phase transition of black holes in the $AdS_5 \times \mathbb{S}^5$ geometry have been treated by considering the number of D3-branes as a thermodynamical variable [22]. Such investigations have been extended to M-theory on $AdS_{p+2} \times \mathbb{S}^{11-(p+2)}$ geometries where $p = 2$ and 5 [23–25]. Precisely, the associated phase transition and stabilities have been investigated by computing certain thermodynamical quantities including the Gibbs free energy and the chemical potential. Motivations to consider such higher dimensional frameworks are associated with non-local objects being useful to understand the AdS/CFT conjecture. In particular, explicit examples of such a correspondence are elaborated in many places including [26]. With progress of string theory, considered as a candidate for a quantum theory of gravity, such optical tools could provide signs of concrete insight and experimental laboratory of the underlying quantum models.

More recently, the shadows and other optical behaviors of the black holes in higher dimensional space-times, motivated by supergravity models, have been extensively investigated. More precisely, 5D black holes involving more than one rotating parameter have been approached using the shadow analysis. A special attention has been devoted to Myers-Perry solutions [27]. The shape and the size of the corresponding shadows have been examined and compared with four dimensional solutions. In particular, it has been found that larger values of the rotation parameter decrease the size.

The aim of this work is to further advance in the study of properties as the shadows of 5D black holes embedded in type IIB superstring geometries. In particular, we consider solutions without and with rotations. Among other results, we find that the shapes are significantly distorted and the sizes are decreasing with the increase of the D3-brane number and the rotating parameter. The geometrical observables and the energetic aspects are also analyzed in some details.

This work is structured as follows. In section 2, we give a fast review on 5D black holes being embedded in type IIB superstring theory. In section 3, we study the shadows of non-rotating black holes in terms of the D3-branes. In section 4, we investigate a 5D black hole with a single rotating parameter. The geometrical observables and the energetic emission aspects are analyzed in section 5. The last section is devoted to conclusions and open questions.

2. 5D rotating type IIB stringy black holes

Let us consider 5D black holes embedded in a type IIB superstring/supergravity geometry with D3-branes. The physics of such solitonic objects has been extensively studied in connections with the AdS/CFT conjecture [28–30]. Properties like the thermodynamical aspects of 5D black holes in such backgrounds have been dealt with by examining certain phase transitions including the Hawking-Page one. Here, we will be interested in optical aspects of such black holes in the $AdS_5 \times \mathbb{S}^5$ physical space. This can be considered as the near horizon geometry of black D3-branes in ten dimensions. Rotating 5D black hole solutions, in general, involve two rotation parameters related to the Casmir operators of the $SO(5)$ Lie group. In this way, non-trivial optical properties depend on such parameters. Following to [30], the metric of a 5D black hole with two rotating parameters assumed to be embedded in the $AdS_5 \times \mathbb{S}^5$ geometry can be written, using Boyer-Lindquist coordinates, as

$$
\begin{aligned}
ds^2 = &-\frac{\Delta_r}{\rho^2}\left(dt - \frac{a\sin^2\theta}{\Xi_a}d\phi - \frac{b\cos^2\theta}{\Xi_b}d\psi\right)^2 + \frac{\rho^2}{\Delta_\theta}d\theta^2 + \frac{\Delta_\theta \sin^2\theta}{\rho^2}\left(adt - \frac{(r^2+a^2)}{\Xi_a}d\phi\right)^2 \\
&+\frac{(1+r^2/\ell^2_{AdS})}{r^2\rho^2}\left(abdt - \frac{b(r^2+a^2)\sin^2\theta}{\Xi_a}d\phi - \frac{a(r^2+b^2)\cos^2\theta}{\Xi_b}d\psi\right)^2 \\
&+\frac{\rho^2}{\Delta_r}dr^2 + \frac{\Delta_\theta\cos^2\theta}{\rho^2}\left(bdt - \frac{(r^2+b^2)}{\Xi_b}d\psi\right)^2 + \ell^2_{AdS}d\Omega_5^2,
\end{aligned}
\tag{2.1}
$$

where the involved terms are

$$
\begin{aligned}
&\rho^2 = r^2 + a^2\cos^2\theta + b^2\sin^2\theta, \\
&\Xi_a = 1 - \frac{a^2}{\ell^2_{AdS}}, \quad \Xi_b = 1 - \frac{b^2}{\ell^2_{AdS}}, \\
&\Delta_r = \frac{1}{r^2}(r^2+a^2)(r^2+b^2)(1+\frac{r^2}{\ell^2_{AdS}}) - m,
\end{aligned}
$$

$$\Delta_\theta = 1 - \frac{a^2}{\ell_{AdS}^2}\cos^2\theta - \frac{b^2}{\ell_{AdS}^2}\sin^2\theta. \tag{2.2}$$

The quantity m is a mass parameter and a and b are the two rotation parameters. The two angular coordinates ϕ and ψ are constrained by $0 \leq \phi \leq 2\pi$ and $0 \leq \psi \leq \pi/2$. $d\Omega_5^2$ is the metric of the five dimensional sphere $\mathbb{S}^5$. From the type IIB superstring/supergravity point of view, the associated ten dimensional factorized spacetime can be interpreted as the near horizon geometry of N coincident configurations of the D3-branes. The AdS radius ℓ_{AdS} and the gravitational constant can be related to N via the following relations

$$\ell_{AdS}^4 = \frac{\sqrt{2}N\ell_p^4}{\pi^2}, \qquad G_5 = \frac{\ell_p^8}{\pi^3\ell_{AdS}^5} = \frac{\ell_p^3}{2^{\frac{5}{8}}\sqrt{\pi}N^{\frac{5}{4}}}. \tag{2.3}$$

It is noted that the metric Eq. (2.1) is singular when $g_{rr} = \Delta_r = 0$ and $\rho^2 = 0$. This metric is invariant under the following symmetry

$$a \leftrightarrow b, \quad \theta \leftrightarrow \frac{\pi}{2} - \theta, \quad \phi \leftrightarrow \psi. \tag{2.4}$$

For the sake of simplicity and to make contact with known results, we will limit our analysis in this work to two cases: zero ($a = b = 0$) and one rotation parameter ($b = 0$). A more general study will be the object of further investigations left for future works.

3. Shadows of 5D non-rotating black holes in presence of D3-branes

Let us study the null geodesics (test "photon" orbits) around such stringy type IIB black holes. We consider first a baseline case with no rotation. In this case $a = b = 0$, the line element in Eq. (2.1) reduces to

$$ds^2 = -\Delta_r dt^2 + \frac{1}{\Delta_r}dr^2 + r^2\left(d\theta^2 + \sin^2\theta d\phi^2 + \cos^2\theta d\psi^2\right) + \ell_{AdS}^2 d\Omega_5^2, \tag{3.5}$$

where Δ_r is a redefined radial function given by

$$\Delta_r = 1 - \frac{m}{r^2} + \frac{r^2}{\ell_{AdS}^2}. \tag{3.6}$$

The integration constant m is related to the black hole mass M through the relation

$$m = \frac{8}{3\pi}G_5 \times M, \tag{3.7}$$

where G_5 is the 5D gravitational constant. It is convenient to consider a normalized mass parameter $m' = \frac{3\pi}{4}m$. In this way, the above metric becomes

$$\Delta_r = 1 - \frac{2G_5 M}{r^2} + \frac{r^2}{\ell_{AdS}^2}. \tag{3.8}$$

In order to implement the D3-brane effect, Eq. (3.8) can be rewritten as (using Eq. (2.3))

$$\Delta_r = 1 - \frac{2^{\frac{3}{8}}M\ell_p^3}{N^{\frac{5}{4}}\sqrt{\pi}r^2} + \frac{\pi r^2}{2^{\frac{1}{4}}N^{\frac{1}{2}}\ell_p^2}. \tag{3.9}$$

The "photon" orbits or null geodesics of the 5D non-rotating black hole geometry can be computed by using an effective Hamilton-Jacobi approach (see [31,32], for example, for more detailed calculations). The corresponding Hamilton-Jacobi equation for the present is

$$\frac{1}{2}g^{\mu\nu}\frac{dS}{dx^\mu}\frac{dS}{dx^\nu} + \frac{dS}{d\tau} = 0, \tag{3.10}$$

where τ is an affine parameter, and where S is the Jacobian action being given by

$$S = -Et + L_\phi\phi + L_\psi\psi + S_r(r) + S_\theta(\theta). \tag{3.11}$$

E, L_ϕ and L_ψ are conserved quantities corresponding to the energy and the angular momentums of the "photon", respectively [31]. It is noted that S_r and S_θ are functions of r and θ only, respectively.

Let us exploit a variable separation method to solve Eq(3.10). Although the use of this method is not strictly necessary in the non-rotating case, it is convenient here to make contact with the rotating case. Separating functions of r and θ, from Eq. (3.10) and Eq. (3.11), we get

$$r^2\Delta_r\left(\frac{dS_r(r)}{dr}\right)^2 - \frac{r^2E^2}{\Delta_r} + L_\psi^2 + L_\phi^2 = -\mathcal{K} \tag{3.12}$$

$$\left(\frac{dS_\theta(\theta)}{d\theta}\right)^2 + L_\phi^2\cot^2\theta + L_\psi^2\tan^2\theta = \mathcal{K}, \tag{3.13}$$

where $\mathcal{K}$ is a (real) constant being interpreted as the Carter constant and considered as an additional constant of motion [32]. According to the Hamilton-Jacobi method, we find the following set of equations

$$\frac{dt}{d\tau} = \frac{E}{\Delta_r}, \tag{3.14}$$

$$r^2 \frac{dr}{d\tau} = \pm\sqrt{\mathcal{R}}, \tag{3.15}$$

$$r^2 \frac{d\theta}{d\tau} = \pm\sqrt{\Theta}, \tag{3.16}$$

$$\frac{d\phi}{d\tau} = \frac{L_\phi}{r^2 \sin^2\theta}, \tag{3.17}$$

$$\frac{d\psi}{d\tau} = \frac{L_\psi}{r^2 \cos^2\theta}, \tag{3.18}$$

where the terms $\mathcal{R}$ and Θ are given, respectively, by

$$\mathcal{R} = -\Delta_r r^2 \left(\mathcal{K} + L_\phi^2 + L_\psi^2\right) + E^2 r^4 \tag{3.19}$$

$$\Theta = \mathcal{K} - L_\phi^2 \cot^2\theta - L_\psi^2 \tan^2\theta. \tag{3.20}$$

To get the shadow boundaries, the expression of the effective potential V_{eff} for a radial motion will be needed. Using the relation

$$\left(\frac{dr}{d\tau}\right)^2 + V_{eff} = 0, \tag{3.21}$$

we obtain the effective potential in such a type IIB stringy solution

$$V_{eff} = \frac{\Delta_r}{r^2}\left(\mathcal{K} + L_\phi^2 + L_\psi^2\right) - E^2. \tag{3.22}$$

The unstable circular orbits relying on the maximum of the effective potential are determined by imposing the following constraints

$$V_{eff} = \frac{dV_{eff}}{dr}\Big|_{r=r_0} = 0, \qquad \mathcal{R} = \frac{d\mathcal{R}}{dr}\Big|_{r=r_0} = 0. \tag{3.23}$$

Eq. (3.9) can be developed to provide

$$\frac{dV_{eff}}{dr}\Big|_{r=r_0} = -2\frac{\left(\mathcal{K} + L_\phi^2 + L_\psi^2\right)\left(N^{\frac{5}{4}}\sqrt{\pi} r^2 - 2^{\frac{11}{8}} M \ell_p^3\right)}{N^{\frac{5}{4}}\sqrt{\pi} r^5} = 0, \tag{3.24}$$

where r_0 is the unstable photon orbit radius. The calculation gives

$$r_0 = \sqrt{\frac{2^{\frac{11}{8}} M \ell_p^3}{N^{\frac{5}{4}} \pi^{\frac{1}{2}}}}. \tag{3.25}$$

Introducing the impact parameters

$$\xi_1 = \frac{L_\phi}{E} \qquad \xi_2 = \frac{L_\psi}{E} \qquad \eta = \frac{\mathcal{K}}{E^2}, \tag{3.26}$$

we find the following algebraic geometrical relation

$$E^2 r_0^2 - E^2\left(\eta + \xi_1^2 + \xi_2^2\right)\left(1 - \frac{2^{\frac{3}{8}} M \ell_p^3}{N^{\frac{5}{4}}\sqrt{\pi} r_0^2} + \frac{\pi r_0^2}{2^{\frac{1}{4}} N^{\frac{1}{2}} \ell_p^2}\right) = 0. \tag{3.27}$$

Using Eq. (3.25), this relation can be reformulated as follows

$$\eta + \xi_1^2 + \xi_2^2 = \frac{2^{\frac{19}{8}} M \ell_p^3 \sqrt{N}}{N^{\frac{7}{4}}\sqrt{\pi} + 2^{\frac{17}{8}} \pi M \ell_p}, \tag{3.28}$$

being a two-dimensional shadow geometry. However, to visualize the corresponding black hole shadows, we introduce the celestial coordinates [33]. Taking the limit of a far away observer, we use such coordinates, considered as a function of the constant of motion

$$\alpha = \lim_{r_O \to +\infty} -r_O^2 \left(\sin\theta \frac{d\phi}{dr} + \cos\theta \frac{d\psi}{dr}\right), \tag{3.29}$$

$$\beta = \lim_{r_O \to +\infty} r_O^2 \frac{d\theta}{dr}, \tag{3.30}$$

where r_O denotes the distance between the black hole and the observer. Using the expressions

$$\frac{dr}{d\tau} = E\sqrt{1 - \frac{\Delta_r\left(\eta + \xi_1^2 + \xi_2^2\right)}{r^2}}, \qquad \frac{d\theta}{d\tau} = \frac{\sqrt{\mathcal{K} - L_\phi^2 \cot^2\theta - L_\psi^2 \tan^2\theta}}{r^2}, \tag{3.31}$$

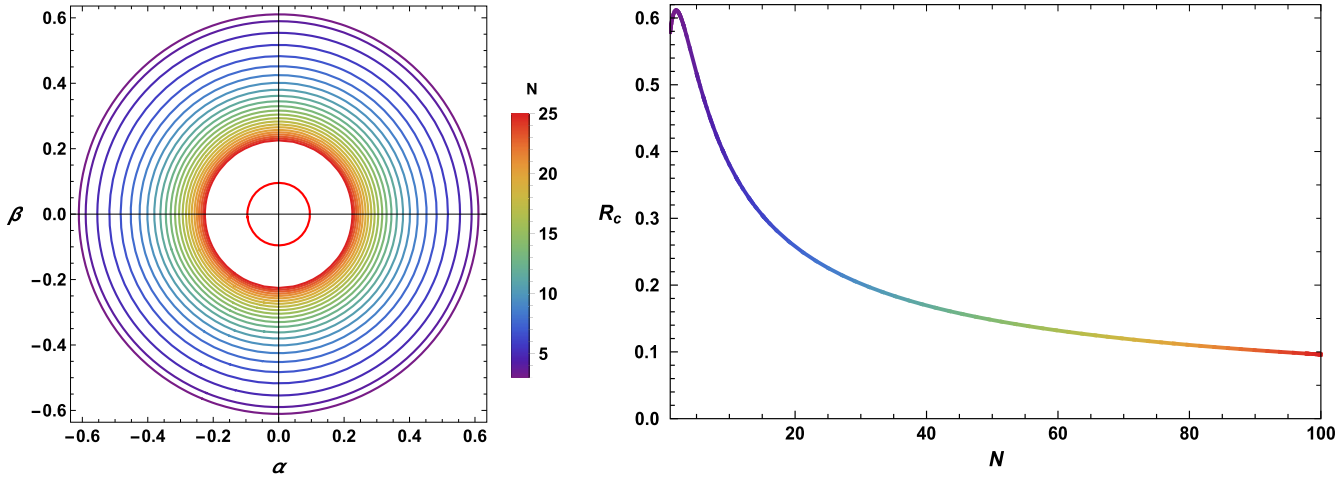

Fig. 1. Left: Black hole shadow in the celestial plane $(\alpha - \beta)$ for different values of the brane number N and $\ell_p = 1, M = 1$. Right: The variation of the shadow radius in terms of the branes number N. In the left panel, the red circle corresponds to the brane number (N = 100).

we get, for these coordinates, the relations

$$\alpha = -\left(\frac{\xi_1}{\sin\theta} + \frac{\xi_2}{\cos\theta}\right), \tag{3.32}$$

$$\beta = \pm\sqrt{\eta - \xi_1^2\cot^2\theta - \xi_2^2\tan^2\theta}. \tag{3.33}$$

Let us study some particular solutions for the sake of illustration. For instance, we can consider the case when an observer is situated in the equatorial hyperplane in 5D, where the inclination angle is $\theta_0 = \frac{\pi}{2}$ and $\xi_2 = 0$. Concretely, the shadow geometry for a 5D non-rotating black hole, in the presence of N D3-branes, is characterized by the relation

$$\alpha^2 + \beta^2 = \eta + \xi_1^2 = \frac{2^{\frac{19}{8}} M\ell_p^3\sqrt{N}}{N^{\frac{7}{4}}\sqrt{\pi} + 2^{\frac{17}{8}}\pi M\ell_p}. \tag{3.34}$$

To inspect the D3-brane effect, we discuss the shadow behaviors and their radius R_c as a function of the D3-brane number N. An examination shows that the D3-brane number can be considered a real parameter controlling the involved size. It can be seen clearly that the shadow shape is circular, while the size decreases by increasing the brane number from a maximum value

$$R_c^{max} = \frac{2\sqrt[7]{2}\,5^{5/7}M^{2/7}\ell_p^{16/7}}{7\pi^{6/7}}, \tag{3.35}$$

at

$$N^{max} = \frac{2\,2^{11/14}\pi^{2/7}M^{4/7}\ell_p^{4/7}}{5^{4/7}}. \tag{3.36}$$

The radius decreases with the D3-brane number and it goes to zero in large N limit. In particular, this could also be seen directly from the metric function Δ_r. This dependence on the brane number is similar to the one of black hole properties obtained recently in M-theory scenarios [34]. We present a illustration of the results in this non-rotating case in Fig. 1.

Having examined the non-rotating black hole shadows with parallel D3-brane configurations, we will focus in the next section on a more general case by taking into account the rotation effect.

4. Shadows of 5D rotating black holes

We go now beyond the previous results by implementing a single rotating parameter. Taking $b = 0$ for simplicity, the line element of a 5D black solution reduces to

$$ds^2 = -\frac{\Delta_r}{\rho^2}\left(dt - \frac{a}{\Xi_a}\sin^2\theta d\phi\right)^2 + \rho^2\left(\frac{dr^2}{\Delta_r} + \frac{d\theta^2}{\Delta_\theta}\right) + r^2\cos^2\theta d\psi^2 \tag{4.37}$$
$$+ \frac{\Delta_\theta\sin^2\theta}{\rho^2}\left(adt - \frac{r^2+a^2}{\Xi_a}d\phi\right)^2 + \ell_{AdS}^2 d\Omega_5^2,$$

where one has now the following reduced terms

$$\Delta_r = (r^2+a^2)(1+\frac{r^2}{\ell_{Ads}^2}) - m, \qquad \Delta_\theta = 1 - \frac{a^2}{\ell_{AdS}^2}\cos^2\theta, \tag{4.38}$$

$$\rho^2 = r^2 + a^2\cos^2\theta, \qquad \Xi_a = 1 - \frac{a^2}{\ell_{AdS}^2}. \tag{4.39}$$

Using the same Hamilton-Jacobi formalism as in the previous section, we get the following variable separated relations

$$\Delta_r\left(\frac{dS_r}{dr}\right)^2-\frac{\left[E(a^2+r^2)-aL_\phi\,\Xi_a\right]^2}{\Delta_r}+\frac{\left(L_\phi\,\Xi_a-aE\right)^2}{\Delta_\theta}+L_\psi^2\left(1+\frac{a^2}{r^2}\right)=-\mathcal{K} \tag{4.40}$$

$$\Delta_\theta\left(\frac{dS_\theta}{d\theta}\right)^2+\cos^2\theta\left(\frac{L_\phi^2\,\Xi_a^2}{\sin^2\theta}-a^2E^2\right)+L_\psi^2\tan^2\theta=\mathcal{K}, \tag{4.41}$$

where the notation is the same as in the previous section. Then, we obtain the geodesic equations

$$\rho^2\frac{dt}{d\tau}=\frac{(r^2+a^2)\left[E(r^2+a^2)-aL_\phi\,\Xi_a\right]}{\Delta_r}+\frac{a(L_\phi\,\Xi_a-aE\sin^2\theta)}{\Delta_\theta}, \tag{4.42}$$

$$\rho^2\frac{dr}{d\tau}=\pm\sqrt{\mathcal{R}}, \tag{4.43}$$

$$\rho^2\frac{d\theta}{d\tau}=\pm\sqrt{\Theta}, \tag{4.44}$$

$$\rho^2\frac{d\phi}{d\tau}=\Xi_a\left[\frac{Ea(r^2+a^2)-a^2L_\phi\,\Xi_a}{\Delta_r}+\frac{Ea\sin^2\theta-L_\phi\,\Xi_a}{\sin^2\Delta_\theta}\right], \tag{4.45}$$

$$\frac{d\psi}{d\tau}=\frac{L_\psi}{r^2\cos^2\theta}, \tag{4.46}$$

where $\mathcal{R}$ and Θ are now given by

$$\Theta=E^2\left[\Delta_\theta\left(\eta-\xi_2^2\tan^2\theta\right)-\cos^2\theta\left(\frac{\xi_1^2\,\Xi_a^2}{\sin^2\theta}-a^2\right)\right], \tag{4.47}$$

$$\mathcal{R}=E^2\left[\left(a^2+r^2-a\xi_1\,\Xi_a\right)^2-\Delta_r\left(\frac{(a-\xi_1\,\Xi_a)^2}{\Delta_\theta}+\eta+\frac{(r^2+a^2)}{r^2}\xi_2^2\right)\right]. \tag{4.48}$$

For $\theta=\frac{\pi}{2}$ and $\psi=\frac{\pi}{2}$ requiring $\xi_2=0$, we find immediately the impact parameters

$$\eta=\frac{r^2\left[16a^2\Delta_r-\left(r\Delta_r'-4\Delta_r\right)^2\right]}{a^2\Delta_r'^2}|_{r=r_0}, \tag{4.49}$$

$$\xi_1=\frac{(a^2+r^2)\Delta_r'-4r\Delta_r}{a\Delta_r'\,\Xi_a}|_{r=r_0}, \tag{4.50}$$

where we have used $\Delta_r'=\frac{\partial\Delta_r}{\partial r}$. Exploiting the previous expressions, these impact parameters take the following form

$$\eta=\frac{4\mu\left(a^2-\mu\right)-r^4\left(a^2\nu-1\right)^2+4r^2\left(a^2\mu\nu+\mu\right)}{\left(a^3\nu+2a\nu r^2+a\right)^2}, \tag{4.51}$$

$$\xi_1=\frac{a^4\nu+a^2\nu r^2-a^2+2\mu-r^2}{a^3\lambda\nu+a\lambda+2a\lambda\nu r^2}, \tag{4.52}$$

where μ, ν, and λ are given by

$$\mu=\frac{2^{3/8}\,\ell_p^3\,M}{\sqrt{\pi}\,n^{5/4}},\qquad \nu=\frac{\pi}{2^{1/4}\,\ell_p^2\,n^{1/2}},\qquad \lambda=1-\frac{\pi a^2}{2^{1/4}\,\ell_p^2\,n^{1/2}}. \tag{4.53}$$

To visualize the associated shadows, we need to introduce the celestial coordinates. For the present model, they are modified as follows

$$\alpha=-\left(\frac{\xi_1}{\sin\theta}+\frac{\xi_2}{\cos\theta}\right), \tag{4.54}$$

$$\beta=\pm\sqrt{\eta-\xi_1^2\cot^2\theta-\xi_2^2\tan^2\theta+a^2\cos^2\theta}. \tag{4.55}$$

In the equatorial plane $\theta=\frac{\pi}{2}$, these celestial coordinates reduce to

$$\alpha=-\xi_1, \tag{4.56}$$

$$\beta=\pm\sqrt{\eta}. \tag{4.57}$$

A close inspection of Eqs. (4.51), (4.52) reveals that the D3-brane number impose strong constraints on the rotating parameter. The possible range of the values of it depends on such a number N. This behavior is illustrated in Fig. 2 where the parametric curves $(\alpha(r),\beta(r))$ are shown for a set of fixed parameters a and N. To get significant shadows as functions of the rotation parameter a, we should consider N lower than a certain number (less than ≈ 8 in the case of the illustrating figure). Fixing the D3-brane number, one observes that the

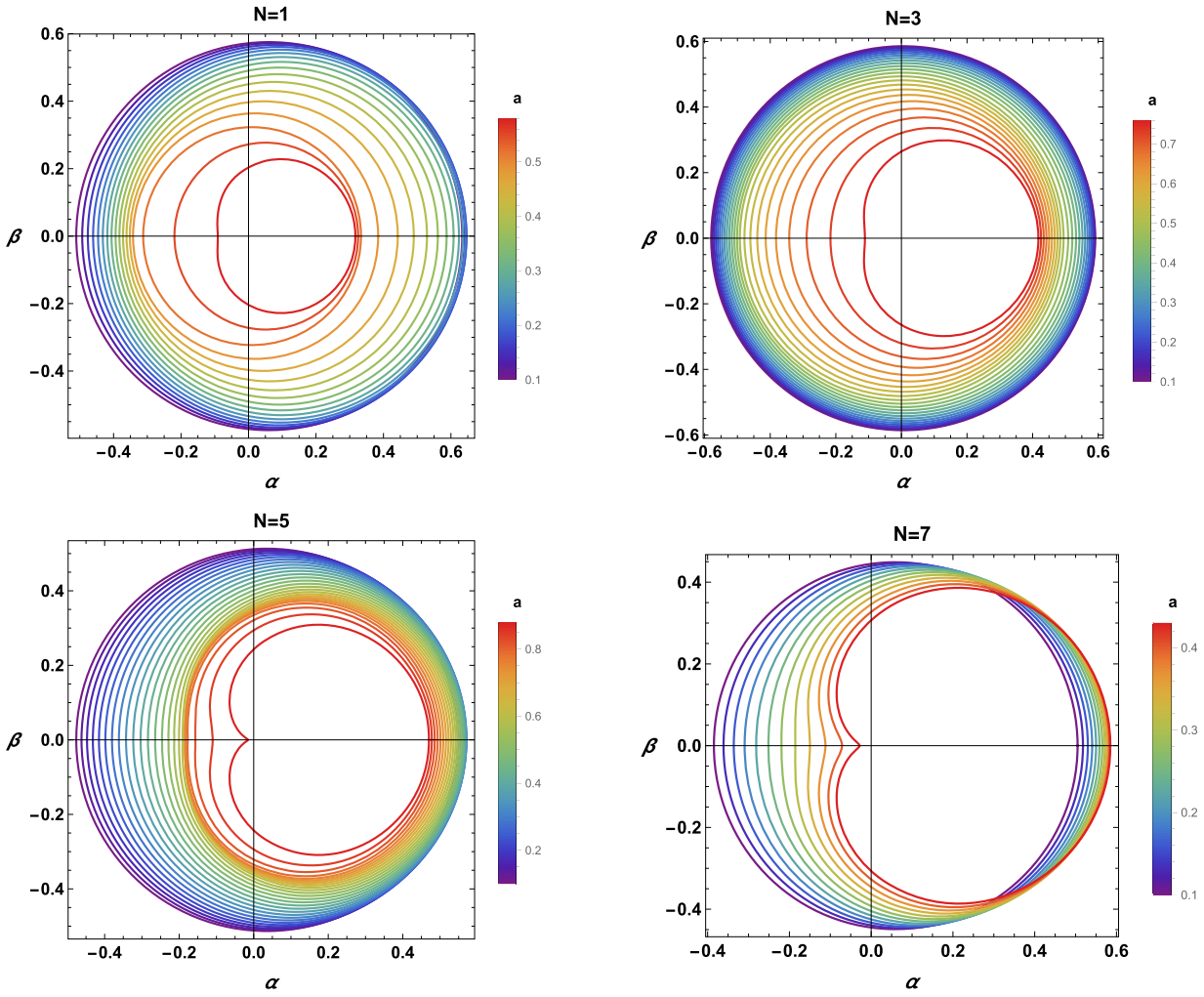

Fig. 2. Shadow geometry of a rotating AdS black hole for different values of the brane number N and the rotating rate a (for $\ell_p = 1$ and $M = 1$).

shadow size decreases by increasing the rotating parameter a. For $N = 1$, the shadows keep the circular behaviors for small values of a. For $N > 1$, however, the shadow starts developing a D-form for the high values of the rotation parameter near $a \simeq 0.7$. As the number of the D3-branes increases the D-shape becomes of "cardioid" type. Similar effects were firstly uncovered in [19]. This complicated geometry has been shown to appear either in M-theory scenarios in the presence of the M2-branes [34] or in charged rotating black holes with a cosmological constant [19]. Let us finally note that the black hole shadow is controlled basically by three parameters (M, N, a) namely a moduli space. Not all regions in such a space are acceptable.

Motivated by the fact that the cosmological parameter deforms the radius of the photon sphere whose radius governs the geometry of the shadow, it is not surprising to find similar results associated with the effect of the D3-brane in stringy black holes. To visualize such behaviors, we plot the shadow geometry, in Fig. 3, can be illustrated in a three dimensional space including a. It follows from this figure that for $N = 1$ and $a < 0.5$, the shadow shape remains circular. While, for $a > 0.5$, the size and the shape of the shadow are modified. Similar aspects are observed for $N = 7$ and $a < 0.3$ where the shadow size remains almost constant keeping a circular configuration. However, for $a > 0.3$, the shape is modified involving the same size. This shows that the D3-brane number can be considered as a relevant parameter controlling the optical properties of black holes on AdS geometries. In addition, we expect that more physical insights could be brought by help of the holographic image of the black holes on AdS backgrounds using dual field theories.

5. Geometrical observable and energy emission rate aspects

In this section, we discuss further geometrical observables and the behavior of the black hole energy emission rate as a function of the brane number and the rotation. The observation of the shadow of the supermassive black hole $M87^{\star}$ has opened a promising to probe gravity theories beyond GR, in particular candidates to quantum gravity as M-theory [34] or string theory (as in the present work). We show next that the present or near-future observational data is indeed sensitive to stringy brane effects, i.e. through N, the number of D3-branes, and, it potentially could be used to put constraints on the black hole parameters and then on the string theory itself.

Geometrical physical observables

We approach now the study of observables which can be useful for making contact with present or future black hole observations. To get geometrical physical data, one needs two observables. They are for example the radius R_c of the shadow and the distortion δ controlling the size and shape respectively. Before going ahead, let us briefly recall the definition of them. To facilitate the discussion, we

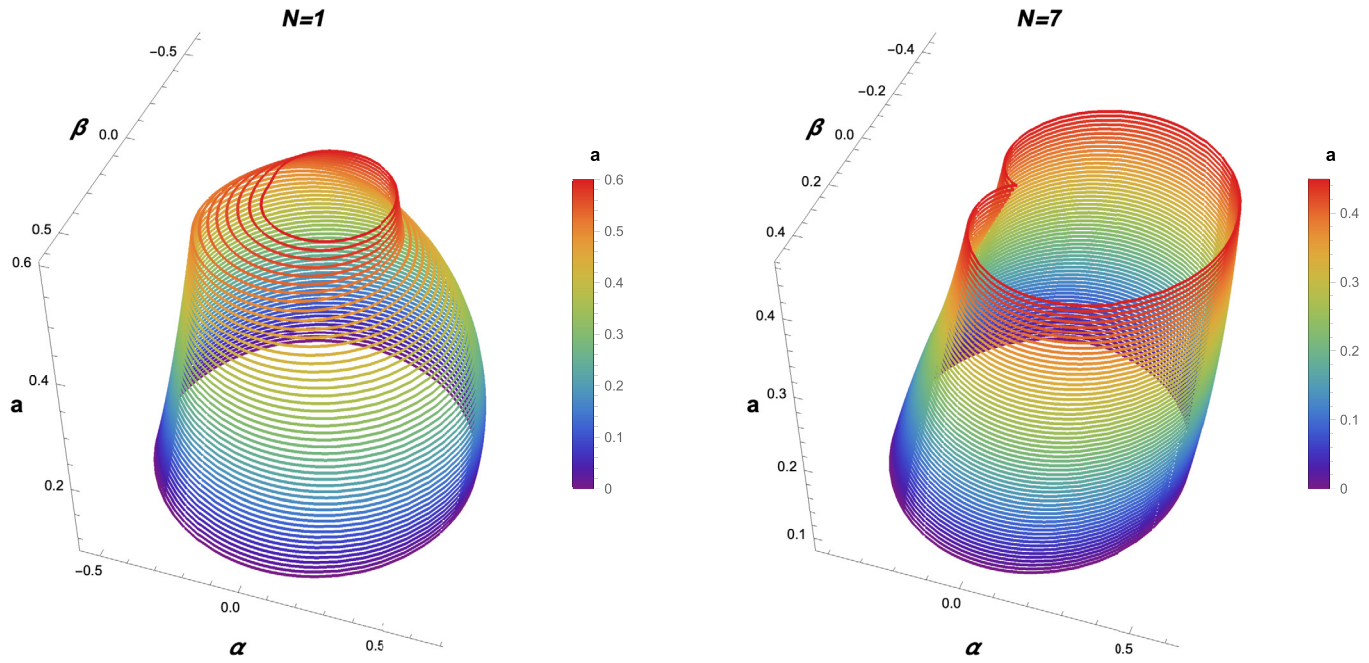

Fig. 3. D3-brane effect on the size and the shape of the shadow for $\ell_p = 1$ and $M = 1$.

consider shadow configurations with $\xi_2 = 0$ as in the previous section. Following [35], the shadow of the black hole is characterized by three specific points. They are the top and the bottom positions (α_t, β_t), (α_b, β_b) respectively, and the point of a standard circle $(\alpha_p, 0)$. The point of the distorted shadow circle $(\alpha_p, 0)$ intersects the horizontal axis at α. The distance between the two points is controlled by the parameter

$$D_c = 2R_c - (\alpha_r - \alpha_p). \tag{5.58}$$

Following to [36], it has been shown that the parameter R_c of shadows takes the following form

$$R_c = \frac{(\alpha_t - \alpha_r)^2 + \beta_t^2}{2|\alpha_t - \alpha_r|}. \tag{5.59}$$

The distortion parameter is characterized by the ratio of D_c and R_c

$$\delta_c = \frac{D_c}{R_c}. \tag{5.60}$$

These geometrical quantities will be discussed graphically. The associated calculations are illustrated in Fig. 4.

One observes from the figure that, at fixed brane number N, the size of the shadow R_c decreases by the increase of the rotation parameter a. For the distortion parameter, however, δ_c increases by increasing the rotation parameter a. It is also noted that δ_c is almost null for $N \simeq 3$. When fixing the rotation a, the quantity R_c increases with the D3-brane number to reach a maximum and then it decreases. However, the distortion parameter δ_c decreases to reach a vanishing value then it increases gradually within increasing N. As it is shown in the previous section, both parameters R_c and δ_c are not always defined and are sensible to a selective value of the moduli space spanned by the triplet (M, N, a).

Energy emission rates

Here, we focus on the energy emission rate. Indeed, for a far distant observer the high energy absorption cross section approaches to the geometrical optical limit, the black hole shadow. In intermediate regimes, the absorption cross section of the black hole oscillates around limiting constant value σ_{lim} at very high energy [37,38]. This limiting constant value, being approximately equal to the size of "photon" 3-sphere. In this approximation, the energy emission rate can be written as

$$\frac{d^2E(\omega)}{d\omega dt} = \frac{2\pi^2\sigma_{lim}}{e^{\frac{\omega}{T_{out}}} - 1}\omega^4, \tag{5.61}$$

where ω is the emission frequency, R_c is the shadow radius and T_{out} is the Hawking temperature of the black hole. In five dimensional space-time, it is recalled that σ_{lim} is approached as

$$\sigma_{lim} \approx \frac{\pi^{3/2}R_c^3}{\Gamma(\frac{5}{2})} \tag{5.62}$$

providing

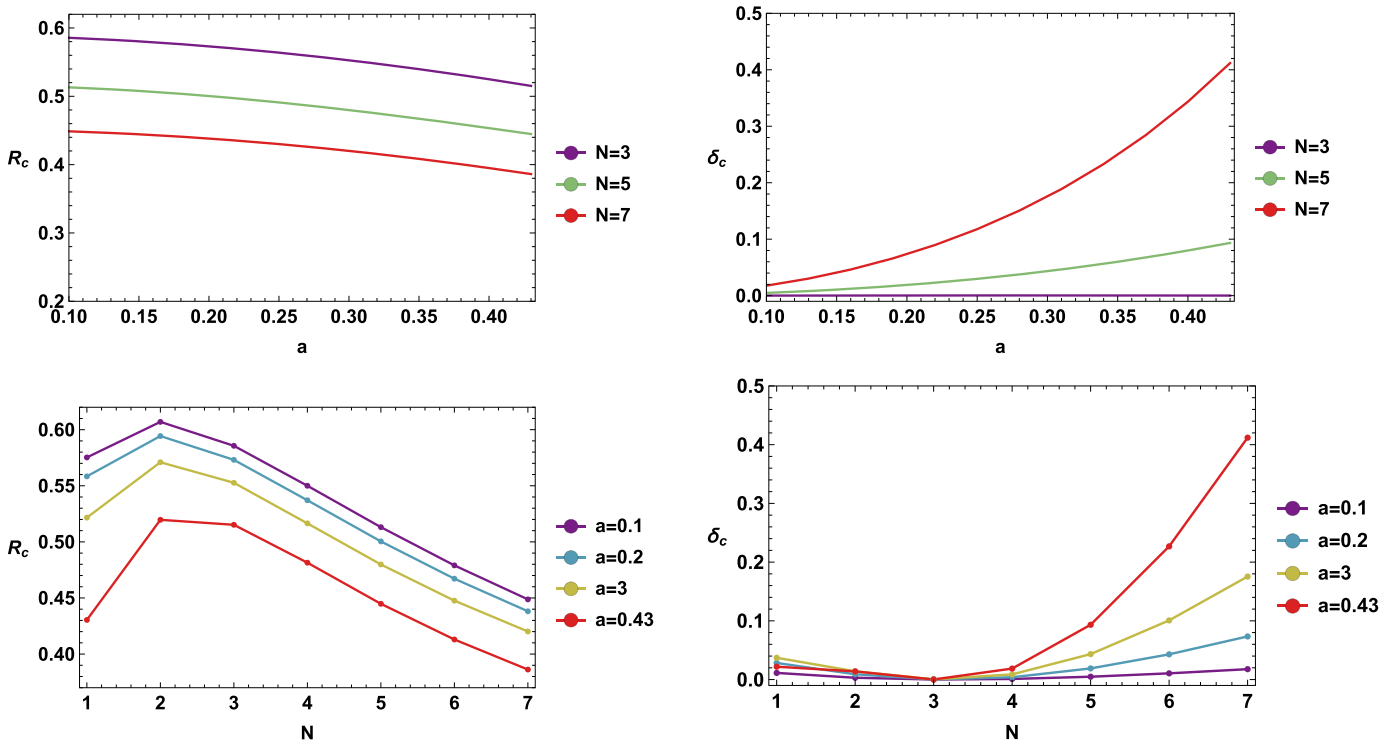

Fig. 4. Astronomical observation variables for different values of the brane numbers N, the rotating rate a, for $\ell_p = 1$ and $M = 1$.

$$\frac{d^2E(\omega)}{d\omega\, dt} = \frac{8\pi^3\, R_c^3}{3(e^{\frac{\omega}{T_{out}}} - 1)}\omega^4. \tag{5.63}$$

In this case, the temperature T_{out} can be expressed as

$$T_{out} = \frac{r_h}{\pi\,(r_h^2 + a^2)}\left(1 + \frac{(2r_h^2 + a^2)}{2^{1/4}\ell_p^2\sqrt{N}}\right), \tag{5.64}$$

where r_h is the horizon radius. We show the illustrate the behavior of the energy emission rate versus the frequency for different values of the rotation parameter and the brane number in Fig. 5.

One observes from the formula, and is graphically clear in Fig. 5, that the energy emission rate varies only slowly. The peak of the energy emission rate slowly shifts to lower frequencies and its height decreases with the increase in the values of the rotation parameter. This behavior is similar to what happens to black holes embedded in M-theory compactifications [34]. Finally we note that increasing the D3-brane number, the energy emission rate vanishes by increasing the rotating parameter.

6. Further discussions and conclusions

In this work, we have investigated the shadow properties of 5D black holes embedded in type IIB superstring/supergravity inspired spacetimes. In particular, we have studied the effect of the presence of an arbitrary number of D3-branes and of the rotation on the shape and size of the shadows. For non-rotating solutions, the circular size of the shadow decreases with the D3-brane number. Larger values of the rotation parameter decrease, however, the size of the shadows. This behavior matches with the "intuitive" idea indicating that when the black hole rotates rapidly, null geodesics or "photon" orbits become closer due to a decreasing in the effective gravitational effects. After that, we have analyzed the geometrical observables associated with the distortion and the size of the shadows, respectively. Among others, we have found that the shapes are significantly more and more distorted and the size is decreasing with the D3-brane number and the rotating parameter. The energy emission rate aspects of such 5D black holes have been examined in some details. It has been remarked that the obtained behavior is similar to the one observed in M-theory black holes [34]. This work opens up for further studies. One interesting question is to complete this analysis by considering the general case where the two rotating parameters supported by the $SO(5)$ Lie symmetry are switched on. In particular, it is interesting to write down the associated shadow geometries. A natural question concerns the extension of this work to the case of external sources involving either dark energy or dark matter. We hope to report elsewhere on these open questions in future.

Declaration of competing interest

The authors declare that they have no known competing financial interests or personal relationships that could have appeared to influence the work reported in this paper.

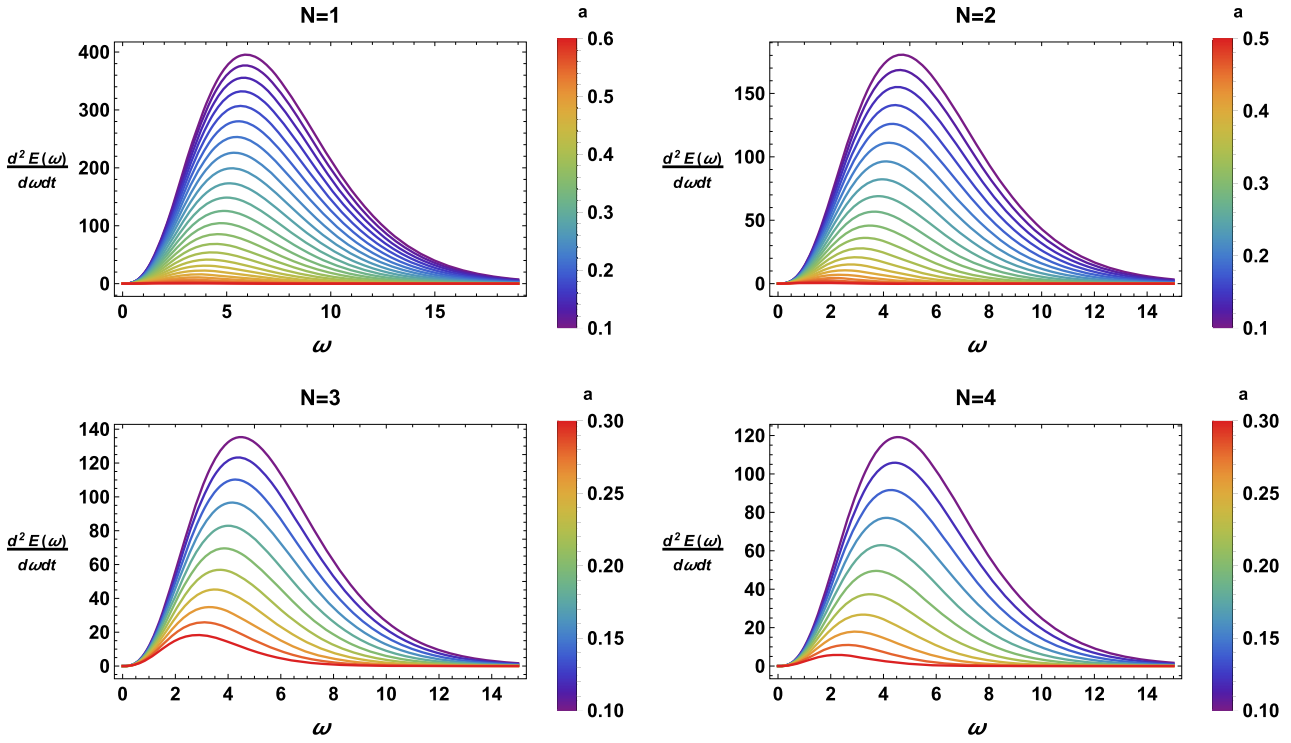

Fig. 5. Emission rate of the $AdS_5 \times \mathbb{S}^5$ black hole for different values of the rotation parameter a and the brane numbers N, for $\ell_p = 1$ and $M = 1$.

Acknowledgements

AB would like to thank the Departamento de Física, Universidad de Murcia for very kind hospitality. The authors would like to thank N. Askor, A. El Balali, S-E. Ennadifi, P. Diaz, J. J. Fernández-Melgarejo, M. P. Garcia del Moral, Y. Hassouni, K. Masmar, M. B. Sedra and A. Segui for discussions on related topics. The work of ET has been supported in part by the Spanish Ministerio de Universidades and Fundacion Seneca (CARM Murcia) grants FIS2015-3454, PI2019-2356B and the Universidad de Murcia project E024-018. This work is partially supported by the ICTP through AF-13.

References

[1] B. Abbott, et al., Observation of gravitational waves from a binary black hole merger, Phys. Rev. Lett. 116 (6) (2016) 061102, arXiv:1602.03837.
[2] K. Akiyama, et al., First M87 event horizon telescope results. IV. Imaging the central supermassive black hole, Astrophys. J. Lett. 4 (1) (2019) 875, arXiv:1906.11241.
[3] K. Akiyama, et al., First M87 event horizon telescope results. V. Imaging the central supermassive black hole, Astrophys. J. Lett. 5 (1) (2019) 875.
[4] K. Akiyama, et al., First M87 event horizon telescope results. VI. Imaging the central supermassive black hole, Astrophys. J. Lett. 6 (1) (2019) 875.
[5] K. Jusufi, M. Azreg-Aïnou, M. Jamil, S.W. Wei, Q. Wu, A. Wang, Quasinormal modes, quasiperiodic oscillations and shadow of rotating regular black holes in non-minimally coupled Einstein-Yang-Mills theory, arXiv:2008.08450.
[6] X.C. Cai, Y.G. Miao, Quasinormal modes of the generalized Ayón-Beato–García black hole in scalar-tensor-vector gravity, Phys. Rev. D 102 (8) (2020) 084061, arXiv:2008.04576.
[7] J. Badía, E.F. Eiroa, Influence of an anisotropic matter field on the shadow of a rotating black hole, Phys. Rev. D 102 (2) (2020) 024066, arXiv:2005.03690.
[8] K. Jusufi, M. Jamil, T. Zhu, Shadows of Sgr A* black hole surrounded by superfluid dark matter halo, Eur. Phys. J. C 80 (5) (2020) 354, arXiv:2005.05299.
[9] D. Kubiznak, R.B. Mann, P-V criticality of charged AdS black holes, J. High Energy Phys. 1207 (2012) 033.
[10] S. Hawking, D.N. Page, Thermodynamics of black holes in anti-De Sitter space, Commun. Math. Phys. 87 (1987) 577.
[11] A. Chamblin, R. Emparan, C. Johnson, R. Myers, Charged AdS black holes and catastrophic holography, Phys. Rev. D 60 (1999) 064018.
[12] A. Belhaj, M. Chabab, H. El Moumni, M.B. Sedra, On thermodynamics of AdS black holes in arbitrary dimensions, Chin. Phys. Lett. 29 (2012) 100401.
[13] P.V. Cunha, C.A. Herdeiro, E. Radu, H.F. Runarsson, Shadows of Kerr black holes with and without scalar hair, Int. J. Mod. Phys. D 25 (2016) 1641021.
[14] K.S. Virbhadra, G.F. Ellis, Schwarzschild black hole lensing, Phys. Rev. D 62 (8) (2000) 084003.
[15] P.-C. Li, M. Guo, B. Chen, Shadow of a spinning black hole in an expanding universe, Phys. Rev. D 101 (8) (2020) 084041.
[16] S-F. Yan, C. Li, L. Xue, X. Ren, Y-F. Cai, D.A. Easson, Y-F. Yuan, H. Zhao, Testing the equivalence principle via the shadow of black holes, Phys. Rev. Res. 2 (2020) 023164, arXiv:1912.12629.
[17] A. Belhaj, A. El Balali, W. El Hadri, M.A. Essebani, M.B. Sedra, A. Segui, Kerr-AdS black hole behaviors from dark energy, Int. J. Mod. Phys. D 29 (09) (2020) 2050069.
[18] C. Goddi, et al., BlackHoleCam: fundamental physics of the galactic center, Int. J. Mod. Phys. D 26 (4) (2016) 1730001, arXiv:1606.08879.
[19] A. Belhaj, M. Benali, A. El Balali, W. El Hadri, H. El Moumni, Shadows of charged and rotating black holes with a cosmological constant, arXiv:2007.09058, 2020.
[20] B. Indrani, C. Sumanta, S. Soumitra, Silhouette of M87*: a new window to peek into the world of hidden dimensions, Phys. Rev. D 101 (4) (2020) 041301, arXiv:1909.09385.
[21] A. Belhaj, L. Chakhchi, H. El Moumni, J. Khalloufi, K. Masmar, Thermal image and phase transitions of charged AdS black holes using shadow analysis, Int. J. Mod. Phys. A 35 (27) (2020) 2050170, arXiv:2005.05893.
[22] J.L. Zhang, R.G. Cai, H. Yu, Phase transition and thermodynamical geometry for Schwarzschild AdS black hole in $AdS_5 \times S^5$ spacetime, J. High Energy Phys. 2 (2015) 143.
[23] A. Belhaj, M. Chabab, H. El Moumni, K. Masmar, M. Sedra, On thermodynamics of AdS black holes in M-theory, Eur. Phys. J. C 76 (2) (2016) 73, arXiv:1509.02196.
[24] M. Chabab, H. El Moumni, K. Masmar, On thermodynamics of charged AdS black holes in extended phases space via M2-branes background, Eur. Phys. J. C 76 (6) (2016) 304, arXiv:1512.07832.
[25] A. Belhaj, A.E. Balali, W.E. Hadri, Y. Hassouni, E. Torrente-Lujan, Phase transitions of quintessential AdS black holes in M-theory/superstring inspired models, arXiv:2004.10647.
[26] A.M. Awad, C.V. Johnson, Higher dimensional Kerr-AdS black holes and the AdS/CFT correspondence, Phys. Rev. D 63 (2001) 124023, arXiv:hep-th/0008211.

[27] P. Uma, A. Farruh, G.G. Sushant, A. Bobomurat, Shadow of five-dimensional rotating Myers-Perry black hole, Phys. Rev. D 90 (2) (2014) 024073, arXiv:1407.0834.
[28] J.M. Maldacena, A. Strominger, E. Witten, Black hole entropy in M theory, High Energy Phys. 1997 (12) (1998) 002, arXiv:hep-th/9711053.
[29] V.R. Alfonso, Introduction to the AdS/CFT correspondence, arXiv:1310.4319.
[30] A.M. Adel, V.J. Clifford, Higher dimensional Kerr-AdS black holes and the AdS/CFT correspondence, Phys. Rev. D 63 (12) (2001) 124023, arXiv:hep-th/0008211.
[31] S. Chandrasekhar, The Mathematical Theory of Black Holes, vol. 69, Oxford University Press, 1998.
[32] B. Carter, Global structure of the Kerr family of gravitational fields, Phys. Rev. 174 (5) (1968) 1559.
[33] M. Amir, B.P. Singh, S.G. Ghosh, Shadows of rotating five-dimensional charged EMCS black holes, Eur. Phys. J. C 78 (5) (2018) 399, arXiv:1707.09521.
[34] A. Belhaj, M. Benali, A.E. Balali, W.E. Hadri, H. El Moumni, E. Torrente-Lujan, Black hole shadows in M-theory scenarios, arXiv:2008.09908 [hep-th].
[35] H. Kenta, K-i. Maeda, Measurement of the Kerr spin parameter by observation of a compact object's shadow, Phys. Rev. D 80 (2) (2009) 024042, arXiv:0904.3575.
[36] A. Muhammed, G.G. Sushant, Shapes of rotating nonsingular black hole shadows, Phys. Rev. D 94 (2) (2016) 024054, arXiv:1603.06382.
[37] S-W. Wei, X-Y. Liu, Observing the shadow of Einstein-Maxwell-Dilaton-Axion black hole, J. Cosmol. Astropart. Phys. 11 (2013) 063, arXiv:1311.4251.
[38] A. Belhaj, M. Benali, A. El Balali, H. El Moumni, S.E. Ennadifi, Deflection angle and shadow behaviors of quintessential black holes in arbitrary dimensions, Class. Quantum Gravity 37 (21) (2020) 215004, arXiv:2006.01078.